Smart Materials and Structures

PURPOSE-LED PUBLISHING™

PAPER • **OPEN ACCESS**

4D printing of reusable mechanical metamaterial energy absorber, experimental and numerical investigation

To cite this article: Ali Fallah *et al* 2025 *Smart Mater. Struct.* **34** 065006

View the article online for updates and enhancements.

You may also like

- Assessment of physio-mechanical characteristics of ABS/PETG blended parts fabricated by material extrusion 3D printing
Vishal Mishra, Nikhil Bharat, Vijay Kumar et al.
- Electroless Plating of NiP and Cu on Polylactic Acid and Polyethylene Terephthalate Glycol-Modified for 3D Printed Flexible Substrates
R. Bernasconi, G. Natale, M. Levi et al.
- Shape memory performance of PETG 4D printed parts under compression in cold, warm, and hot programming
E Soleyman, D Rahmatabadi, K Soltanmohammadi et al.

This content was downloaded from IP address 212.156.75.166 on 07/07/2025 at 06:53

OPEN ACCESS
IOP Publishing
Smart Materials and Structures
Smart Mater. Struct. **34** (2025) 065006 (19pp)
https://doi.org/10.1088/1361-665X/addead

4D printing of reusable mechanical metamaterial energy absorber, experimental and numerical investigation

Ali Fallah[1,2,3,*], **Qandeel Saleem**[1,2,5], **Giulia Scalet**[4] **and Bahattin Koc**[1,2,*]

[1] Integrated Manufacturing Technologies Research and Application Center, Sabanci University, Tuzla, Istanbul 34956, Turkey
[2] Faculty of Engineering and Natural Sciences, Sabanci University, Tuzla, Istanbul 34956, Turkey
[3] Department of Automotive Engineering, Atilim University, Ankara 06830, Turkey
[4] Department of Civil Engineering and Architecture, University of Pavia, via Ferrata 3, 27100 Pavia, Italy
[5] Department of Physics, Durham University, Durham DH1 3LE, United Kingdom

E-mail: ali.fallah@atilim.edu.tr and bahattinkoc@sabanciuniv.edu

Received 23 March 2025, revised 12 May 2025
Accepted for publication 29 May 2025
Published 6 June 2025

Abstract

This study investigates the compression behavior, energy absorption, shape memory properties, and reusability of 4D-printed smart mechanical metamaterials. Four structural configurations, i.e. honeycomb, re-entrant, and two modified re-entrant designs were developed to assess microstructure effects. Samples were fabricated using Polylactic Acid (PLA), a widely used shape memory polymer (SMP) in 4D printing, and polyethylene terephthalate glycol (PETG), an emerging SMP with demonstrated shape memory performance in recent studies. Cold-programming-induced shape recovery was evaluated at room temperature, simulating real-world conditions. Finite element simulations of compression and shape memory cycles matched experimental results well. Auxetic samples with negative Poisson's ratios showed superior energy absorption. However, only PETG demonstrated sufficient reusability, while PLA proved unsuitable for reusable designs. The PETG-3 modified re-entrant structure exhibited the best performance, with high energy absorption, delayed densification onset, and shape recovery and reusability factors of 0.95 and 0.96, respectively. Findings highlight the importance of considering both shape recovery and reusability when designing smart structures to address industrial challenges.

Keywords: 4D printing, smart structures, shape memory polymers, energy absorption

* Authors to whom any correspondence should be addressed.

Original content from this work may be used under the terms of the Creative Commons Attribution 4.0 licence. Any further distribution of this work must maintain attribution to the author(s) and the title of the work, journal citation and DOI.

© 2025 The Author(s). Published by IOP Publishing Ltd

1. Introduction

Energy absorption is the ability of a material or structure to dissipate and absorb energy when exposed to external forces or impacts. In applications where safety and protection are crucial, such as automotive crash structures or sports equipment, the energy absorption capacity of materials is of utmost importance [1–4]. Traditional structures like honeycomb, and sandwich panels, although capable of absorbing energy, are not specifically designed for optimal energy absorption [5]. Auxetic structures, on the other hand, offer several advantages over conventional structures for energy absorption applications. These mechanical meta-materials with a negative Poisson's ratio (NPR) exhibit unique properties that stem from their topology at a smaller scale, allowing for tailored mechanical and physical characteristics [6]. Auxetic materials can undergo significant compressive strains at a nearly constant stress level, enabling them to absorb energy more efficiently and minimize the force transmitted to the surrounding environment. Numerous studies have been conducted to investigate the mechanical behavior and energy absorption of auxetic structures with different unit cell designs, such as re-entrant [7–10], semi-rigid [11–13], and chiral [14, 15], star [16], arrowhead structures [17]. For example, Li *et al* [9] explored the mechanical response of auxetic structures with a re-entrant design under compressive loads. Their research demonstrated that by altering the cell geometry, the mechanical properties and Poisson's ratio of the structure can be modified. Moreover, their findings revealed that structures with an NPR exhibited higher energy absorption and lower transmitted stress compared to structures with a positive Poisson's ratio.

One of the challenges in utilizing auxetic metamaterials is their manufacturability using traditional methods like hot pressing and injection molding. However, recent advancements in additive manufacturing (AM) have enabled the fabrication of structures with complex architectures, leading to increased interest in mechanical metamaterials [18, 19]. Several commonly used thermoplastic materials, including polylactic acid (PLA), acrylonitrile butadiene styrene, Polypropylene, Polyetheretherketone, Polyetherimide, and polyethylene terephthalate glycol (PETG) are now utilized in AM processes [20–22]. These thermoplastics offer numerous advantages, such as versatility, affordability, design freedom, and minimal waste [23–25].

Despite the advantages of 3D printed auxetic structures, they may experience permanent deformation or damage after absorbing energy, necessitating replacement. However, the application of intelligent materials, such as polymer with shape memory effects i.e. shape memory polymers (SMPs), in AM has led to the development of smart products capable of changing shape or volume when exposed to different stimuli, known as 4D printing [26].

Unlike traditional 3D printed structures, 4D printed auxetic structures can recover their original shape after being permanently deformed and be reused again. This reusability feature contributes to a circular economic approach, reduces waste, and promotes sustainability. By minimizing material waste and reducing the need for constant replacement, these structures conserve resources and decrease the overall environmental impact of various industries. Additionally, the potential for reusing 4D printed structures in different applications extends their lifecycle and maximizes their value. Several studies have investigated the energy absorption and shape recovery of 4D printed structures with different configurations [26–28]. For instance, Xin *et al* [28] conducted research on 4D printing chiral metamaterials, aiming to achieve tunable, programmable, and reconfigurable properties. Their study focused on optimizing the tensile properties of the 4D printed structures for potential biomedical applications. By exploring different unit cell configurations, they discovered the ability to tailor the structure properties to match specific tissues or organs. Notably, their 4D printed structures exhibited an impressive shape recovery capability, even after undergoing substantial deformation, reaching up to 90%. Another study by Namvar *et al* [27] explored the energy absorption and shape recovery characteristics of 4D printed auxetic structures. They extensively examined the properties of structures with re-entrant, hexagonal, and AuxHex unit cells through a combination of experimental and numerical analysis. The findings revealed that the re-entrant structures showcased superior energy absorption capabilities compared to the others. Additionally, all the structures demonstrated successful shape recovery at RT.

However, it is worth noting that neither of the aforementioned studies specifically examined the reusability of the recovered structures, which is a crucial aspect to consider in the context of smart energy absorbers. Recently, there have been a few published studies that have focused on investigating the reusability and repeatability of energy absorption in 4D printed structures [29–33]. For example, Sun *et al* [30] explored the repeatable compressive behavior of 4D printed thin-walled corrugated structures. By incorporating a corrugation design, they achieved stable mechanical properties and demonstrated the ability of the structures to undergo repetitive compression and recovery cycles. In another study, Dong *et al* [29] conducted research on the reusability and energy absorption performance of 4D printed fiber-reinforced auxetic structures. Their findings highlighted that 4D printed structures exhibited excellent reusability, with a shape recovery ratio above 90% even after undergoing multiple test cycles. Additionally, these structures maintained significant energy absorption capabilities even after six test cycles. In a recent study, Zhang *et al* [33] studied energy absorption properties of 4D printed structures with different unit cells. Their result proved that the samples produced by PETG have higher reusability compared to those ones fabricated by PLA.

Although the mentioned studies provide valuable insights into the reusability of 4D printed auxetic structures, further investigation is still necessary to gain a deeper understanding of how different parameters such as employed SMPs, and the configuration of the unit cell influence the reusability characteristics of such structures. Besides that, in these studies, the focus is on experimental activities and there is no reliable and accurate computational model to predict the whole

shape memory cycle of the 4D printed structures including the programing and recovery process. This computational model is necessary for the optimization process required for future applications.

It is worth noting that the shape-memory cycle of thermal-sensitive SMPs consists of programming and recovery stages. During the programming stage, the material is deformed from its original shape to a new shape known as the programmed shape. If this process occurs below the switching temperature (T_{SW}), it is referred to as cold programming (CP); if it occurs above T_{SW}, it is referred to as hot programming (HP). The T_{SW} can be either the glass transition temperature (T_g) or melting temperature (T_m) of the SMP [34, 35]. After programming, if the SMP is heated above the T_{SW} range, it will return to its original shape, a process known as recovery [35]. Due to the time and temperature-dependent nature of polymers, it is easy to program SMPs at rubbery or melting temperatures, i.e. using HP. However, HP-based 4D printed structures must be programmed in controlled environmental conditions and the programmed shape must usually be predetermined. These conditions may not be feasible for load-bearing components in real-world applications as there is no control over the environmental conditions and the deformations caused by applied loads [24, 36]. Thus, for load bearing applications, CP-based 4D printed that can be deformed enough at RT without breaking and then recover their original shape are preferred. To address this requirement, in this study CP is utilized to measure the shape memory properties of the 4D printed structures for real industrial applications.

This study focuses on exploring compression behavior, energy absorption, shape memory properties, and reusability of 4D-printed smart auxetic structures. To gain insights into the impact of unit cell shape on the behavior of auxetic structures, four different configurations, including honeycomb, re-entrant, and two modified re-entrant designs, were designed and fabricated. The 4D printed samples were fabricated using commonly used SMPs i.e., PLA and PETG. To simulate real-world conditions, the shape recovery of the 4D printed structures was evaluated through CP-induced shape memory effects at RT. The compression behavior and complete shape memory cycle of the 4D printed structures were simulated using finite element methods, demonstrating good agreement between experimental and numerical findings. The findings suggest that although the samples printed with PLA and PETG show a shape recovery ratio exceeding 90%, the 4D-printed PETG samples demonstrate excellent reusability compared to PLA samples. Furthermore, these samples exhibit a substantial energy absorption capacity even after undergoing two testing cycles.

2. Materials and methods

2.1. Design and fabrication of samples

In the study, four distinct sandwich structures were developed based on unit cell designs, each with different core shapes. These structures were assigned specific numbers for easier identification among the samples. Each structure was crafted with an identical count of unit cells: three cells in the x direction and four in the y direction. As a result, they all maintained a height of 36 mm (y-direction) and a z-direction thickness of 10 mm. The wall thickness for every structure was consistently set at 0.40 mm. Figure 1 presents the unit cell design for each of these four structures. Pattern 2 is identified as the conventional re-entrant auxetic structure with a NPR, while Patterns 1 and 3 are adaptations of this design. Notably, Pattern 1 exhibits a zero Poisson's ratio as it integrates unit cells with both negative and positive Poisson's ratios. Pattern 3, while possessing a NPR, is believed to have enhanced mechanical properties due to its additional vertical struts, distinguishing it from the typical re-entrant design. On the other hand, Pattern 4 employs the well-known honeycomb design and has a positive Poisson's ratio, acting as the reference structure for the study.

For fabrication of structures, two different filaments were procured from eSUN® for this study: PETG filament (diameter: 1.75 mm, density: 1.27 mg mm^{-3}) and PLA filament (diameter: 1.75 mm, density: 1.24 mg mm^{-3}). The 3D structures were printed using a Creality Ender 3 Pro attached with a 0.4 mm nozzle. Printing speed and nozzle temperature were set to 50 mm s^{-1} and 210 °C for PLA and 50 mm s^{-1} and 240 °C for PETG, respectively. The printed samples are referred to as PLA-X or PETG-X which X stands for the pattern used for printing of those samples. Moreover, C1 and C2 are added in the name of samples to show that they have been tested for the first and second cycle, respectively.

2.2. Dynamic mechanical analysis

Dynamic mechanical analysis (DMA) is a useful tool to analyze the thermo-mechanical behavior of SMPs. In addition, it helps to find the temperature at which the SMP transitioned from the glassy state to rubbery state i.e., T_g. The analysis was conducted using Netzsch DMA 242 C analyzer. A sample of length 10 mm, width 3.6 mm, and thickness 0.8 mm was tested using tension as the deformation mode. The analysis was performed within temperatures of 25 °C to 120 °C, at a heating rate of 3 °C min^{-1}, frequency of 1 Hz and applied strain 0.001 mm mm^{-1}.

2.3. Mechanical testing, energy absorption analysis and reusability investigation

In this study, quasi-static uniaxial compression tests were performed using a universal testing machine from ZwickRoell, Germany at RT with constant crosshead speed (5 mm min^{-1}). The stress–strain curves obtained from the compression tests were used to calculate the energy absorption behavior of each sample.

As illustrated in figure 2, a stress–strain curve has three stages: the first stage involves an almost linear increase in stress by increasing the applied strain until micro buckling or cracks starts in the structure. The stress and strain at the end of this linear region are designated by yield stress (σ_y) and yield strain (ε_y), respectively. In the next region, the stress

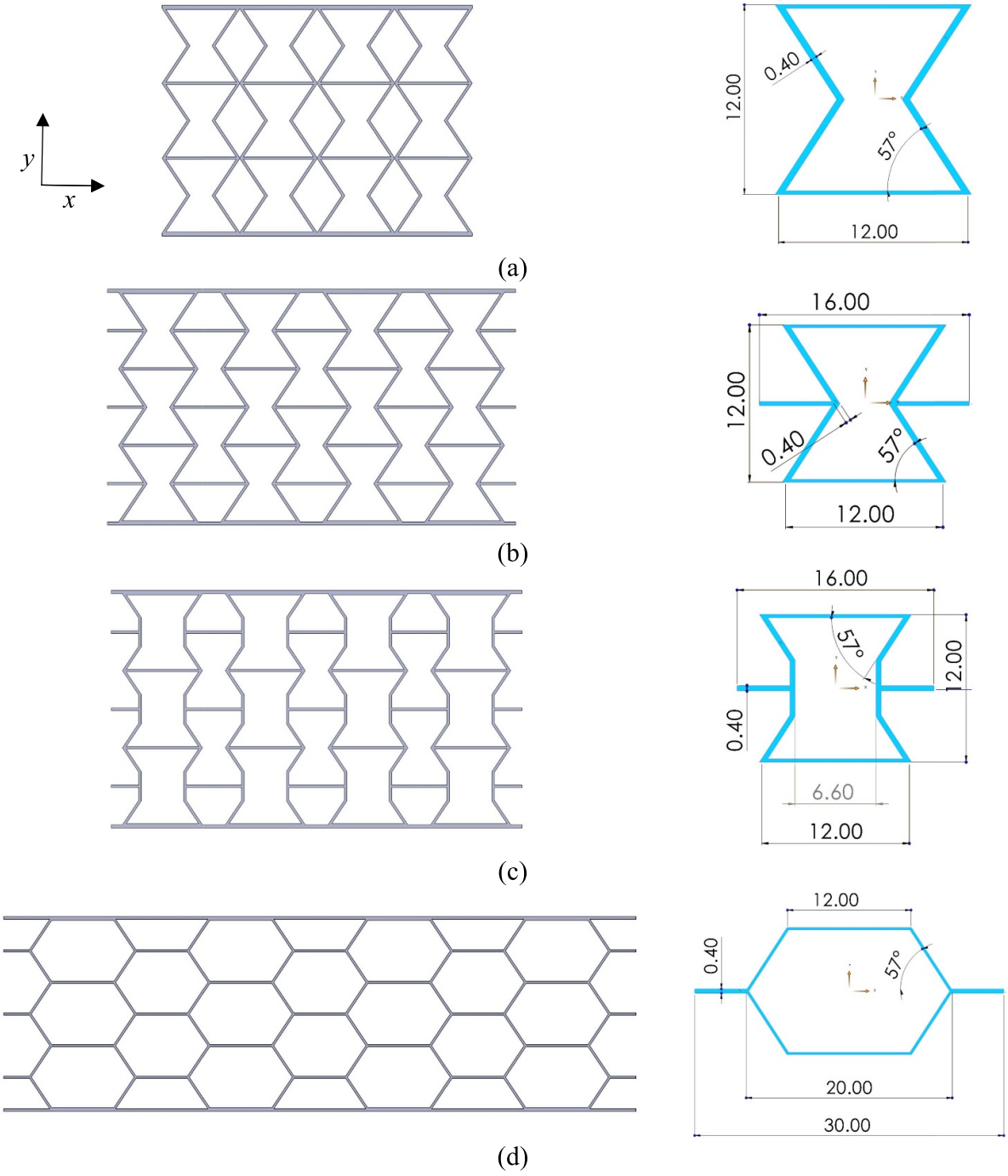

Figure 1. Structural configurations of auxetic core sandwich structures, (a) Pattern 1, (b) Pattern 2, (c) Pattern 3, and (d) Pattern 4.

first increases nonlinearly to reach its maximum value. Then, it decreases until reach to almost constant value for a range of applied strains, which is called plateau region. As the structure is compressed more, it undergoes densification, and stress increases rapidly as the strain value increases. Densification strain (ε_d), is the strain that the densification starts.

To quantify the energy-absorbing capabilities of structures, several metrics have been developed and applied. Volumetric energy refers to the amount of energy dissipated for a given volume (J m^{-3}). It can be computed from a compressive stress–strain curve as [37, 38]

$$E = \int_0^{\varepsilon_f} \sigma d\varepsilon \tag{1}$$

where ε_f is the strain to failure of the sandwich structure. The definition of failure in energy absorbers can vary based on application and thus has been defined as different points along a stress–strain curve. Typically, the stress limit of a practical

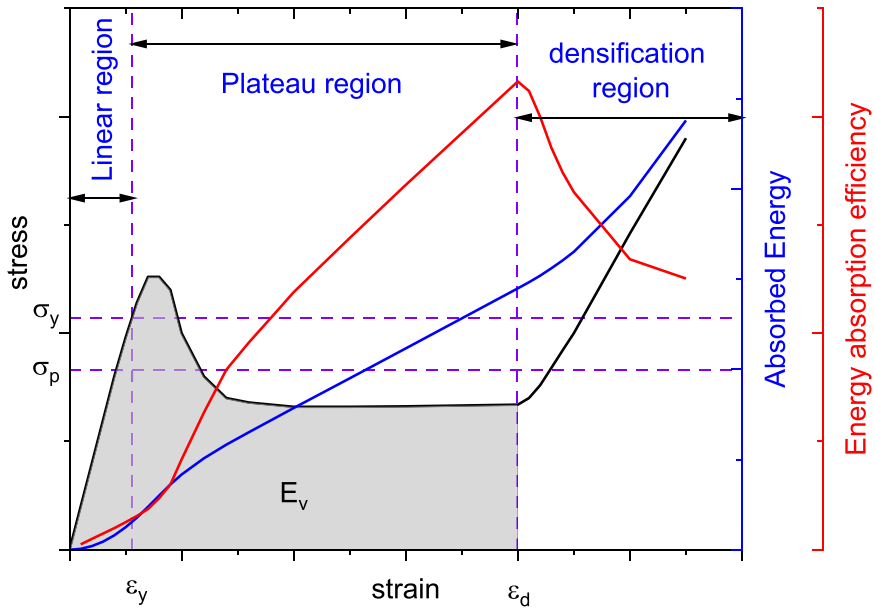

Figure 2. Schematic illustration of a typical force–displacement curve of a lattice material obtained from a cyclic compression test.

energy absorber is defined by the onset of densification (ε_{d}), i.e. $\varepsilon_{\mathrm{f}} = \varepsilon_{\mathrm{d}}$. Among different methods available to determine ε_{d}, here energy efficiency method is used. Based on this method, the energy absorption efficiency, (η), is calculated as the area under a stress–strain curve divided by the instantaneous stress as [39]:

$$\eta\left(\varepsilon_{\mathrm{i}}\right) = \frac{\int_0^{\varepsilon_{\mathrm{i}}} \sigma\left(\varepsilon\right) \mathrm{d}\varepsilon}{\sigma_{\mathrm{i}}} \tag{2}$$

where σ_i is stress at strain ε_{i}. Based on this method, the densification onset, i.e. ε_{d}, is the strain corresponding to the maximum of energy absorption efficiency. After densification starts, the stress and consequently the transmitted force rises swiftly which is not desirable for energy absorption applications since it may lead to damage or system failure. Thus, it is advantageous for the energy absorbing structure to have higher ε_{d} to avoid reaching the densification phase.

The absorbed energy per unit mass i.e. SEA (specific energy absorption) and absorbed energy per unit volume E_{v} were also important indicators in evaluating the energy absorption capacity. The absorbed energy of the tested specimens was calculated up to the onset of densification strain (ε_{d}) as [39]:

$$E_{\mathrm{v}} = \int_0^{\varepsilon_{\mathrm{d}}} \sigma\left(\varepsilon\right) \mathrm{d}\varepsilon \tag{3}$$

$$\mathrm{SEA} = \frac{E_{\mathrm{v}}}{\rho} \tag{4}$$

where ρ is density.

It should be noted that most of the energy was absorbed in the plateau regime. Therefore, the magnitude of plateau stress (σ_{p}) and its length are important parameters in the design of sandwich structures for energy absorption application. The plateau stress of the compressed specimens was calculated as [39]:

$$\sigma_{\mathrm{p}} = \frac{\int_{\varepsilon_{\mathrm{y}}}^{\varepsilon_{\mathrm{d}}} \sigma\left(\varepsilon\right) \mathrm{d}\varepsilon}{\varepsilon_{\mathrm{d}} - \varepsilon_{\mathrm{y}}}. \tag{5}$$

For clarification the defined parameters are shown in the figure 2. Generally, with similar SEA or E_{v}, a structure with longer plateau region is more desirable for energy absorption applications.

2.4. Shape memory test and reusability

The shape memory cycle of thermal-sensitive SMPs consists of programming and recovery stages. During the programming stage, the material is deformed from its original shape to a new shape called the programmed shape. In the recovery stage, the SMP is able to recover its original shape in response to an external stimulus. The shape recovery properties of SMPs differ from the elastic recovery seen in hyper-elastic materials like rubbers. Polymers with shape memory effect are able to memorize the original shape and temporarily maintain a deformed shape. The shape memory properties of SMPs can be quantified using the shape recovery ratio (R_{r}) and shape fixity ratio (R_{f}). An ideal SMP would have $R_{\mathrm{r}} = R_{\mathrm{f}} = 1$, meaning it would maintain its temporary shape and fully recover its original shape during the recovery process. However, real-world SMPs do not behave perfectly, and these ratios are usually less than one. Moreover, in some applications only one of these properties are desired. For example, for a 4D printed energy absorber it is important that it can recover the original shape after being deformed as much as possible and the ability of remembering the temporary shape is not important. Thus, in this study only the shape recovery of 4D printed samples is investigated and reported.

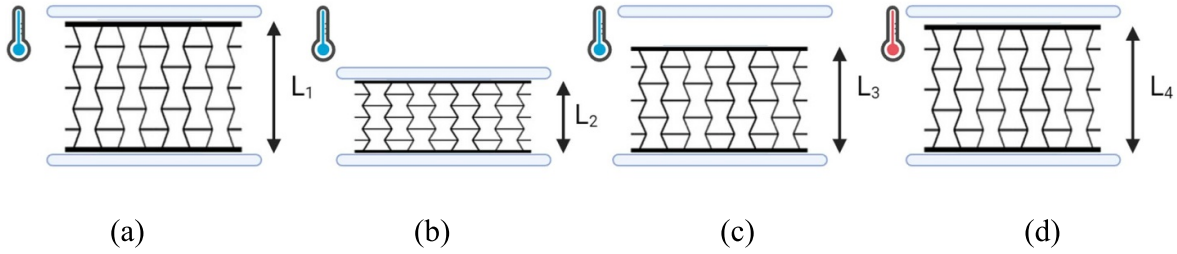

Figure 3. Schematic diagram of parameters used in shape recovery test. (a) Initial configuration, (b) at the end of loading, (c) after unloading, and (d) after recovery.

To study the shape memory behavior of the 4D printed structures, the quasi-static compression test at RT is considered as the programming step. During this step, plastic deformation is induced in the deformed structure and a temporary or programmed shape is obtained. Then, upon heating the structure above the T_g of the polymer, the material recovers the plastic deformation, and such a step is called recovery step. The shape memory test procedure is shown in figure 3. The original dimension of each as-prepared sample L_1 was measured before the compression test. The sample deformed under loading and the dimension became L_2. Upon unloading, the sample recovered some of its previous shape and dimension became L_3, which was considered as the programmed shape. After heating the deformed samples above the T_g of polymer, the final dimensions were measured and labeled as L_4. The R_f and R_r were calculated as:

$$R_f = \frac{L_1 - L_3}{L_1 - L_2} \tag{6}$$

$$R_r = \frac{L_4 - L_2}{L_1 - L_2}. \tag{7}$$

As mentioned earlier, one of the main features of the 4D printed structures is their reusability after recovery step. In other words, a 4D printed structure not only should recover the original shape at the end of recovery test, but also its mechanical performance should be as close as possible to the intact structure. Otherwise, the 4D printed structure is not useful for real industrial applications. To investigate the reusability of the 4D printed structures, here a second cycle of programming and recovery is done. The structure recovered from the first cycle is deformed again under the same conditions and then its recovery and mechanical properties are investigated and compared with the first cycle. Theoretically, the behavior of structure at the second cycle should be equal to the first cycle, however existence of unrecoverable plastic deformation and possible cracks inside the structure led to a lower performance in the second cycle compared to the first cycle. In order to quantify the reusability of the structures, in this study a metric termed reusability factor (RF) is introduced as:

$$\mathrm{RF} = \frac{(E_v)_{C_2}}{(E_v)_{C_1}} \tag{8}$$

where $(E_v)_{C_i}$ is the E_v of the structure at the ith cycle of the compression test. Based on this terminology, if the structure can absorb the same amount of energy as the first cycle in the second one, the $\mathrm{RF} = 1$ and the structure is completely reusable. However, in reality $\mathrm{RF} < 1$ and the structures with higher RF are desirable in terms of reusability.

2.5. Finite element simulation

The mechanical and shape memory behavior of the printed samples are simulated using the commercial finite-element software ABAQUS/Standard. Despite most available studies in literature that only model the loading and unloading steps, here the whole loading, unloading and shape recovery process is simulated.

The structures are meshed using C3D20R elements which are 20-node quadratic brick elements with reduced integration points, while the rigid plate is meshed with R3D4 elements which are 4-node 3D bilinear rigid quadrilateral elements. The appropriate dimensions of the elements were set to be 0.2 mm after the independence of the mesh was examined.

To model the thermo-mechanical behavior of SMPs, the 3D constitutive model developed by Boatti *et al* [40] is used and implemented into the ABAQUS environment using a UMAT subroutine. This model distinguishes rubbery and glassy phases using a rule of mixtures to capture temperature-dependent moduli, phase transformation kinetics, and non-ideal shape-fixing/recovery. Internal state variables track stored strain and phase fractions, ensuring accurate modeling of the loading–unloading–recovery cycle. Model parameters are identified from experimental data, as detailed in section 3.1.

A quasi-static mechanical analysis was performed. Figure 4 shows the applied boundary conditions on the model during the simulation. The 3D structures are fixed (fully constrained along with the three principal directions) at the bottom face. A rigid plate and a reference point are placed on the top face of the structure. To simulate the compression test, a displacement is applied to this reference point downward. Besides, the structure's movement is constrained in the out-of-plane direction to prevent out-of-plane global buckling of the structure under compression. To avoid interpenetration, general contact is defined between the rigid plates and the surfaces. Figure 5

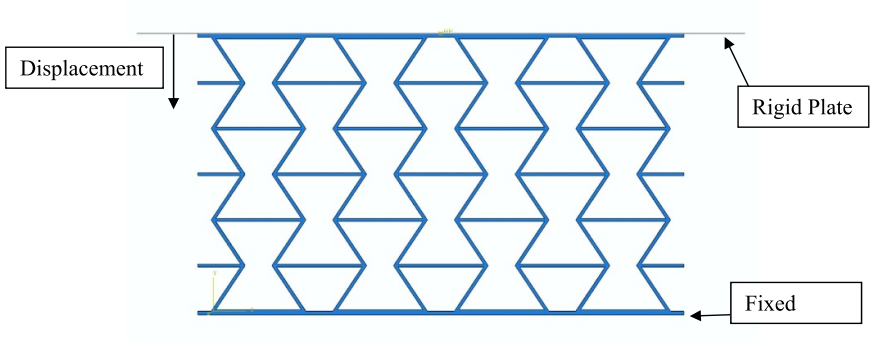

Figure 4. Applied boundary conditions used in finite element simulations.

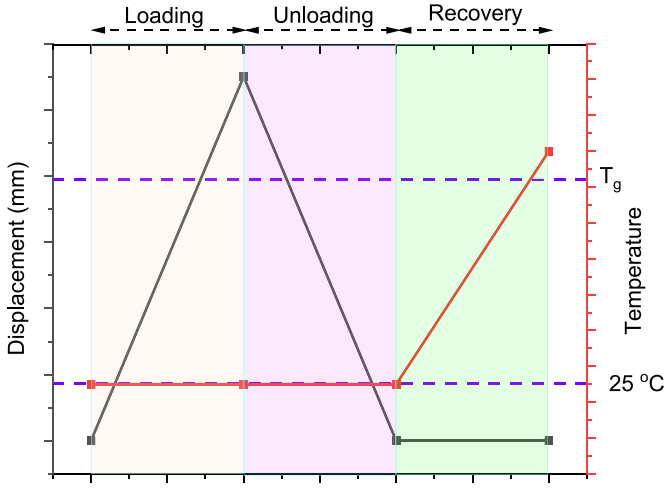

Figure 5. Thermo-mechanical loading conditions applied during the finite element simulation of the shape memory tests of 4D printed structures. A uniform temperature field history is applied.

shows the thermo-mechanical conditions during the whole loading, unloading and recovery steps.

3. Results and discussion

3.1. Thermo-mechanical behavior of PETG and PLA

The DMA curves obtained for PETG and PLA, exhibiting the dynamic storage modulus and loss factor (tan(δ)), are shown in figure 6. DMA is an effective technique to determine the T_g of polymers. Determination of T_g is crucial as SMPs recover their original shape when heated above this temperature. PLA and PETG, being amorphous glassy polymers, undergo glass transition, where a transformation from glassy to rubbery state takes place. Since storage modulus is a temperature-dependent property, it experiences a sharp decrease when T_g is reached. Moreover, at T_g, the tan(δ) reaches its maximum, thus T_g of PETG is found to be 87.01 °C, whereas PLA has a lower T_g of 66.92 °C. Hence, shape memory behavior of PETG and PLA was studied at 90 °C and 70 °C, respectively. Moreover, the result shows that the PLA has higher storage modulus than the PETG.

In order to perform the finite element simulations introduced in section 2.5, the constitutive model parameters used to describe the SMP's thermo-mechanical behavior are first identified. To this end, DMA results are used and the model parameters obtained are shown in table 1. More details about the employed constitutive model and how to extract the parameters and their definition can be found in Boatti *et al* [40].

3.2. Compression test and energy absorption performance

The mechanical and energy absorption properties of 4D printed structures designed with different configurations are investigated using the quasi-static compression test. As mentioned before, auxetic structures, due to their NPR, are known to boost the mechanical properties and energy absorption performance of materials. Here, the effect of both the structural configuration and the material used for the fabrication of the 4D printed structures on their mechanical performance is investigated.

The deformation patterns observed in the PETG and PLA 4D-printed structures under the first cycle of uniaxial compressive loading are shown in figures 7 and 8, respectively. In these figures, the initial configuration, the deformed shape at the end of loading, the deformed shape after unloading and the final shape after shape recovery test are presented for all configurations. Results of finite element simulations are also added for comparison and validation of presented numerical model which are in good agreement with the experimental data.

As can be seen from figures 7(a-ii) and 8(a-ii), the PETG-1 and PLA-1 samples are buckled laterally at the end of loading, which can be attributed to the lack of lateral stiffness. They also bent on one side while being compressed as they did not have any support in the horizontal direction. On the other hand, figures 7(b-ii) and (c-ii), figures 8(b-ii) and (c-ii) show that samples with pattern 2 and 3 exhibited a more stable deformation response owing to the horizontal support these structures had and shrunk inwards [41]. This can be attributed to the NPR of these structures. PLA-4, and PETG-4, which have a conventional honeycomb structure, are also being deformed in a stable manner and due to their positive Poisson's ratio, their expand in the lateral direction (see figures 7(d-ii) and 8(d-ii)). Results also show that the deformation in pattern 4 is much

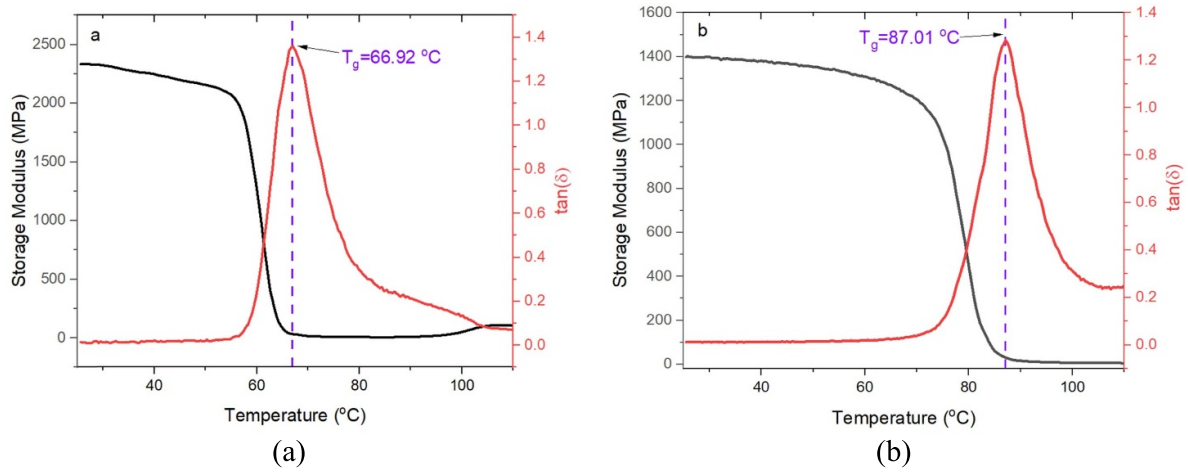

Figure 6. The result of DMA tests of (a) PLA and (b) PETG in terms of storage modulus and tan(δ) versus temperature.

Table 1. Constitutive model parameters used for finite element simulations.

Parameter	PETG	PLA	Units
E^{g}	1400	2270	MPa
E^{r}	1	50	MPa
ν^{r}	0.49	0.49	—
ν^{g}	0.29	0.29	—
R^{pg}	35	20	MPa
h	20	100	MPa
$\Delta\theta$	10	10.0	K
θ_t	87.01	66.92	K
c	0.6	0.67	—
c_p	0.04	0.02	—

more than the other ones, and cracks have been seen in the PLA-4. Since the PLA is more brittle than the PETG, these cracks only happened for PLA samples. These results demonstrate the applicability of structures with either zero or NPR for energy absorption applications.

In figures 7(iii) and 8(iii) the configuration of all the samples after unloading is shown. It is obvious that in all cases, upon unloading, the applied deformation is partially recovered elastically, as plastic strain has been induced in the structures. The configuration at the end of unloading is considered as the temporary shape for the 4D printed structures.

Finally, in figures 7(iv) and 8(iv) the shape of samples after recovery test is presented. As can been seen, all structures recovered their original shape. Details about the shape recovery ratio of the samples will be provided in the coming section.

Moreover, as can be seen, the results of finite element simulations are in good agreement with the experimental results in all loading, unloading and recovery steps. In some parts the predicted deformation using finite element simulations is slightly different from the experimental results which can be due to geometry imperfections during manufacturing (not considered by the finite element model) or limitations in modeling such a complex behavior of the SMPs under investigation (e.g., adopted hyperlastic law, anisotropy). However, besides those local points, the model can simulate the deformation pattern of the structure with adequate accuracy.

Figures 9 and 10 show the stress–strain curve of the first cycle of compression test of the printed PETG and PLA samples, respectively. In these figures, experimental results together with finite element simulation results are presented and, despite few differences, they are in excellent agreement which proves the accuracy of the proposed numerical approach. It should be noted that the offset and difference between the numerical and experimental curves can be due mostly to the defects and imperfectness in printing of samples or foam filling process. Besides that, the employed constitutive model for describing the mechanical behavior of PLA and PETG affects the peaks stress and the plateau region in the stress–strain curve.

These figures show that the stress–strain curve of 4D printed samples not only changes by using different patterns but also by using different materials. As DMA results showed before, PLA has higher mechanical properties compared to PETG, thus in all cases the PLA can tolerate higher stress than the PETG samples. Moreover, in all the curves, three different regions, i.e. linear, plateau and densification, can be observed. However, the length of the plateau region and the beginning of densification vary among the samples considering their geometry and the material used to fabricate them.

Results show that the amount of decrease in the stress value after reaching its maximum value, in the PETG samples are lower than in the PLA ones. This aspect can be attributed to the high flexibility of PETG at RT, which makes the PETG samples flexible enough to deform and withstand loads without cracking or breaking within the structure. While in the PLA samples, as the plateau region starts, the stress decreases swiftly which is not desirable for energy absorption applications. The amount of stress reduction is much more severe in the PLA-4 which has a positive Poisson's ratio that can be considered a sign that these types of structures are not optimal for energy absorption applications.

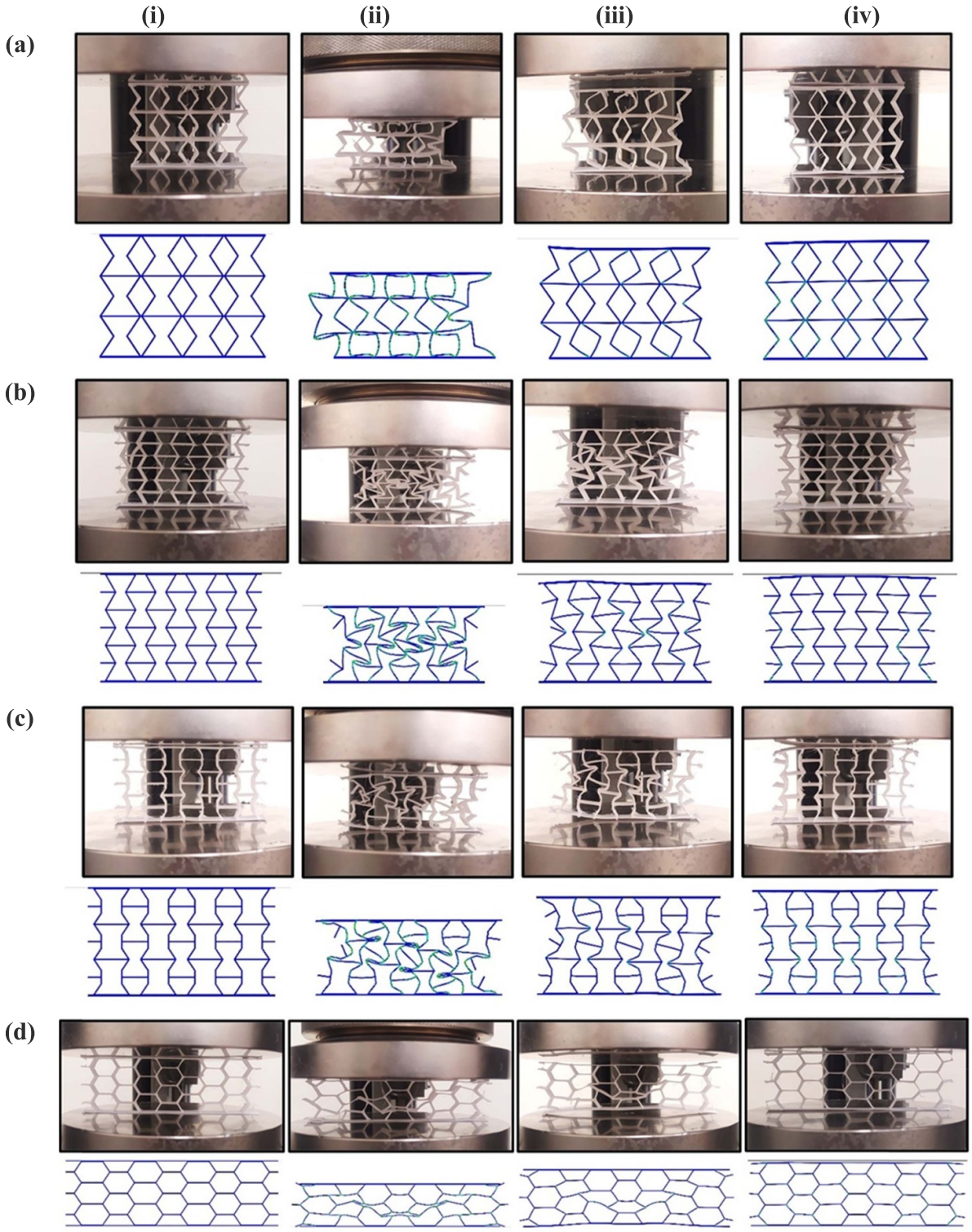

Figure 7. Deformation patterns in the first cycle of compression and shape recovery tests for (a)PETG-1, (b) PETG-2, (c) PETG-3, (d) PETG-4 at (i) initial configuration, (ii) end of compression test, (iii) after unloading, and (iv) after recovery test.

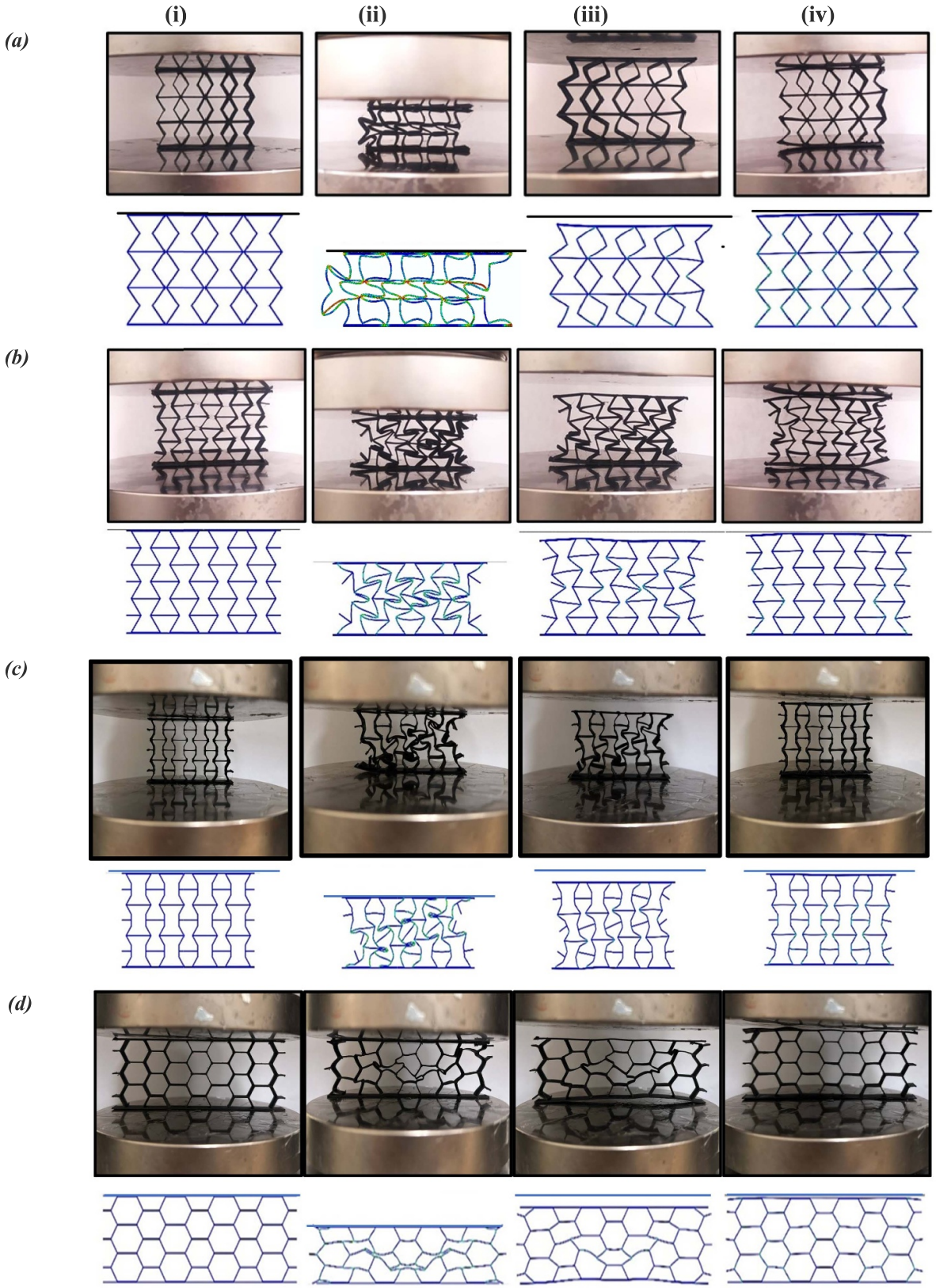

Figure 8. Deformation patterns in the first cycle of compression and shape recovery tests for (a)PLA-1, (b) PLA-2, (c) PLA-3, (d) PLA-4 at (i) initial configuration, (ii) end of compression test, (iii) after unloading, and (iv) after recovery test.

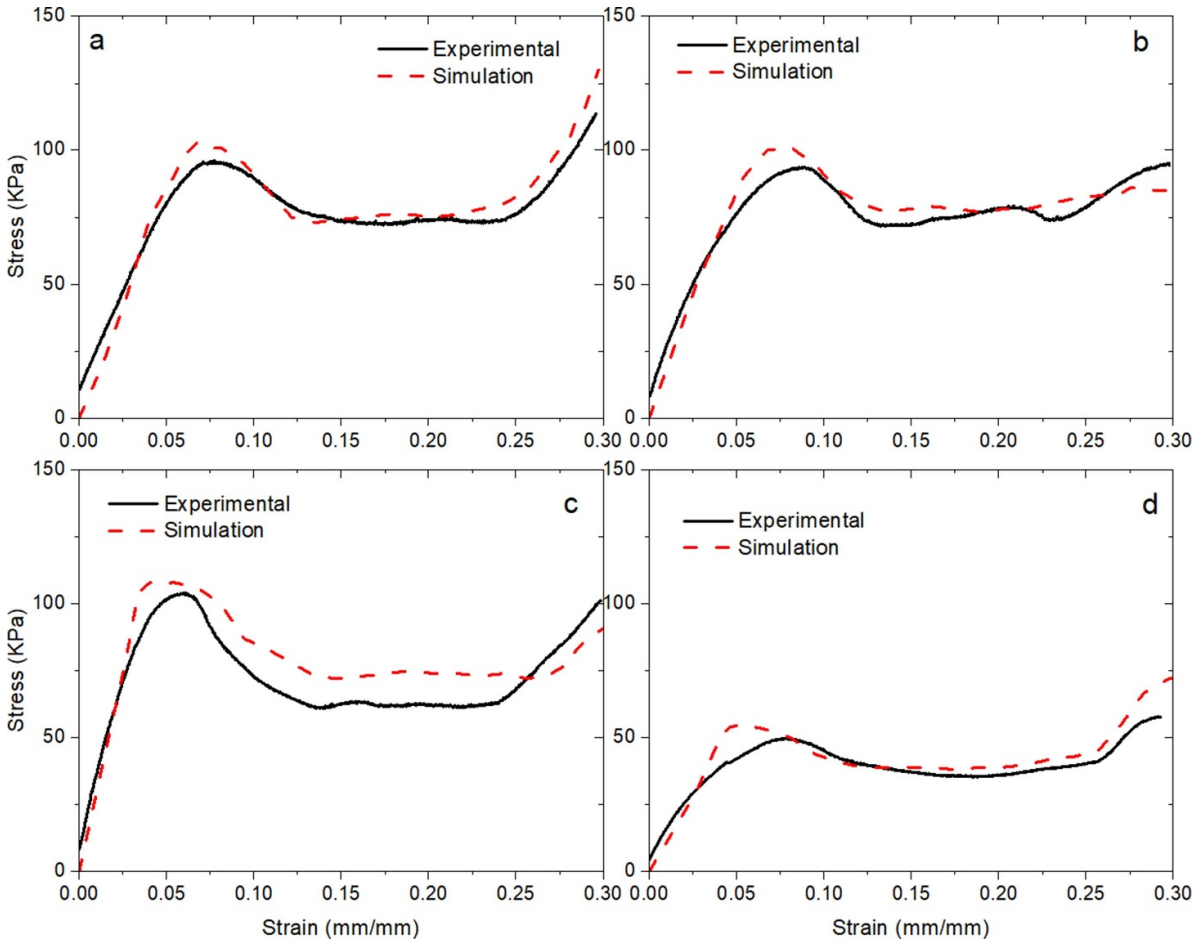

Figure 9. The stress–strain curve of first cycle of compression test for (a) PETG-1, (b) PETG-2, (c) PETG-3, and (d) PETG-4.

Results also show that the onset of densification of PLA-2, PETG-2 and PLA-3 is not easily visible, while PLA-1, PETG-1, PLA-4, and PETG-4 reach this stage and a rapid increase in the transferred stress can been seen in their stress–strain curve. It can be explained by considering that pattern 2 and pattern 3 are auxetic structures with NPR, while pattern 1 and pattern 4 have zero and positive Poisson's ratio, respectively. It proves the applicability of auxetic structures with NPR for energy absorption applications. Moreover, the maximum stress for pattern 3 is higher than pattern 2, which is due to additional vertical struts in pattern 3.

Tables 2 and 3 detail and compare the key energy absorption parameters of both PETGA and PLA 4D-printed structures obtained from the experimental and numerical simulations. To clarify how the corresponding parameters are calculated, the stress–strain curves of PETG-1 and PLA-1 are presented in figure 11. The absorbed energy per volume and the energy absorption efficiency are also plotted in these figures. The main parameters such as ε_d, ε_y, σ_p, and E_v can be easily calculated from these figures.

It should be noted that the E_v plays an important role in determining how efficiently a structure absorbs energy as potential energy absorbers are required to buckle and fail as per the predictions [41]. On the other hand, SEA is a more precise indication of energy absorption as it provides weight efficiency of the crashworthiness of the structure by estimating the E_v per unit mass of the structure. A structure can be deemed a good energy absorber if it has a high SEA value and the difference between the σ_p and σ_y is minimal. Moreover, efficiency is useful in analyzing the uniformity of the crushing loads. A higher efficiency value is desirable for energy absorption applications [42].

Based on the results presented in table 2, among the samples made of PETG, the PETG-2, with NPR have the highest $\varepsilon_d = 0.30$. For the remaining samples, the onset of densification is almost at the same level. In terms of SEA, the PETG-2 has the highest value, i.e. $0.13\frac{kJ}{kg}$, while the PETG-4 has the lowest SAE. Moreover, PETG-2 and PETG-4 have the highest and lowest E_v at the onset of densification, respectively. In terms of efficiency, PETG-3 has the highest value of efficiency at the start of densification. In terms of plateau stress (σ_p) the PETG-4 has the lowest value, which is almost half of the other samples. Considering all these facts, it can be concluded that PETG-2 and PETG-3 with NPR have the best performance, while PETG-4 with positive Poisson's ratio has the worst performance in terms of energy absorption parameters.

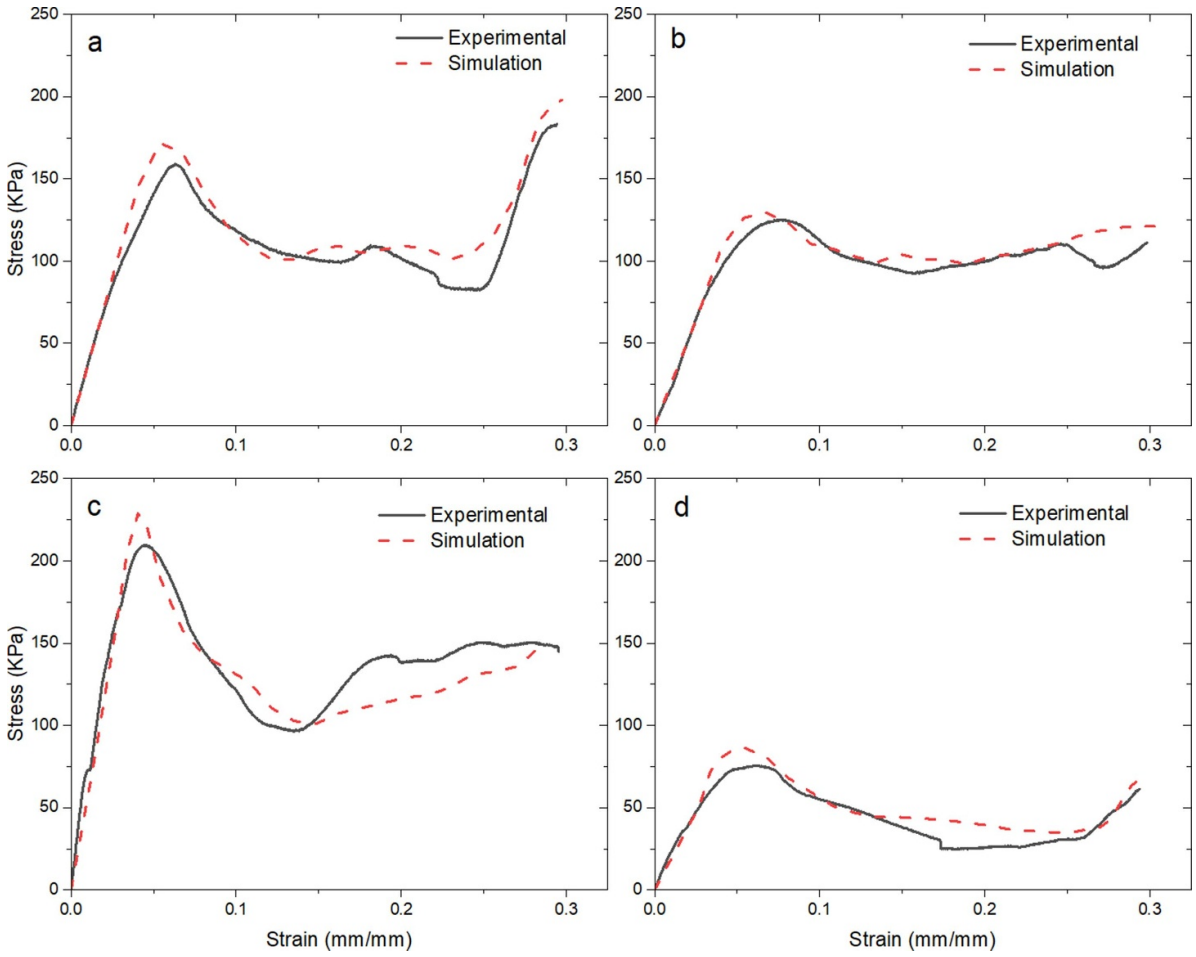

Figure 10. The stress–strain curve of first cycle of compression test for (a) PLA-1, (b) PLA-2, (c) PLA-3, and (d) PLA-4.

Based on the results presented in the table 3, among the samples made of PLA, the PLA-2 and PLA-3, with NPR have the highest ε_d i.e. 0.28 and 0.30, respectively. However, PLA-1 with zero Poisson's ratio has $\varepsilon_d = 0.25$ and the ε_d for PLA-4 with positive Poisson's ratio is 0.22. As mentioned before, in energy absorption applications it is desired to reach densification at higher strains. This result proves again that the auxetic structures with NPR are more desirable in energy absorption application than the structures with positive Poisson's ratio. Moreover, among all the samples, the PLA-3 has the highest SEA $\left(0.22\frac{\text{kJ}}{\text{kg}}\right)$, while the PLA-4 has the lowest one $\left(0.10\frac{\text{kJ}}{\text{kg}}\right)$. Considering the E_v it is obvious that PLA-3 and PLA-1 can absorb more energy before reaching to densification while the PLA-4 has the lowest E_v. These results prove that despite huge usage of conventional honeycomb structures in different fields; they are not optimized in terms of energy absorption properties and the auxetic structures are a better option for this type of application.

Considering the better mechanical properties of PLA compared to PETG, it was expected that PLA samples show higher σ_y, σ_p, SEA, and E_v than the PETG ones. In all cases the numerical and experimental values are in good agreement and the same pattern can be seen in the results.

3.3. Shape memory behavior and reusability of 4D printed structures

The shape memory performance of 4D PETG and PLA structures under CP conditions is presented in figures 7 and 8. As mentioned before, at the during the loading step at RT, the plastic deformation is induced in the structures which led to the temporary shape, see figures 7(iii) and 8(iii). Since the structures were not unloaded immediately, stress relaxation occurred and the SMP chains continued to align along the direction of load, and consequently stored energy. Upon unloading, the structures retained some of their shape due to viscoelastic recovery and stored elastic strain. Then, by immersing the deformed structures in the hot water bath, their shape recovery behavior are investigated, see figures 7(iv) and 8(iv). When the structures were heated above their T_g (90 °C for PETG and 70 °C for PLA), the crystallites in the reversible phase of the SMP melted and the structures

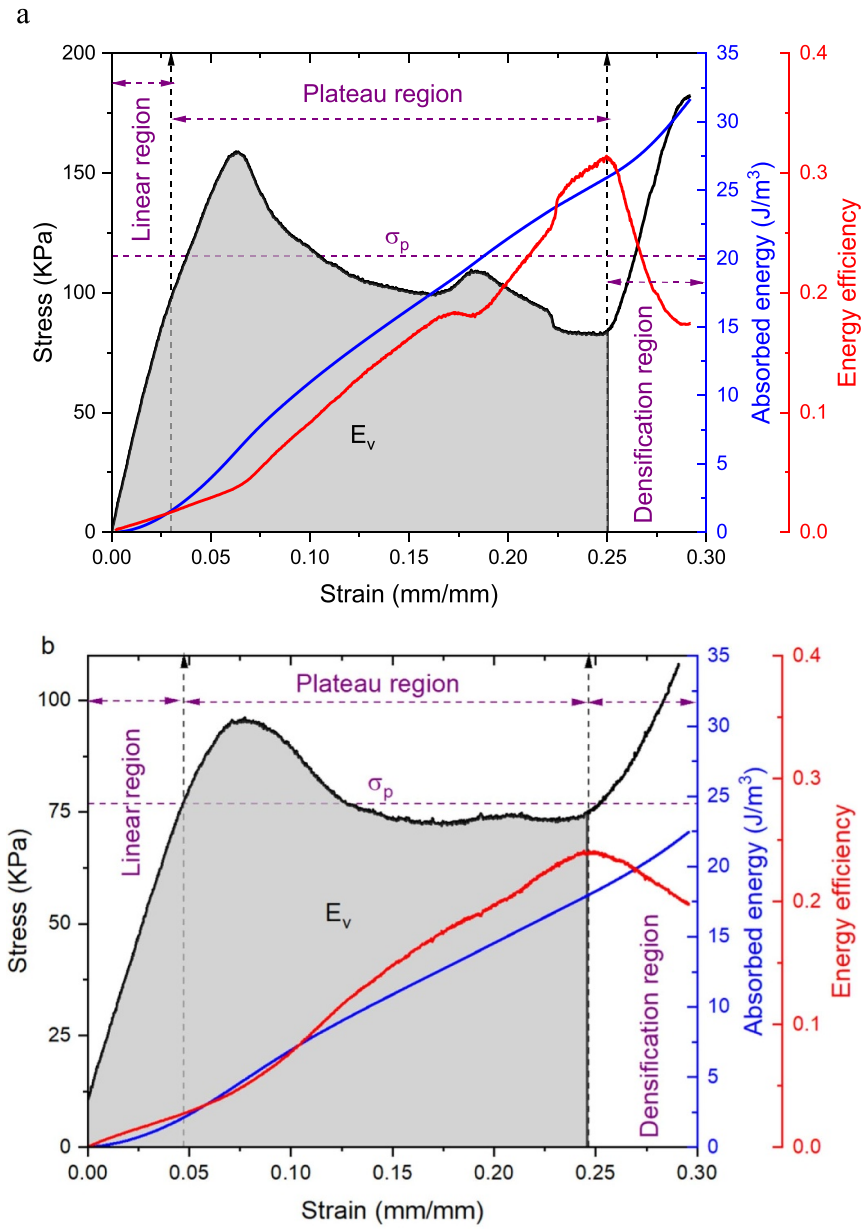

Figure 11. The stress–strain curve, energy absorbed and the efficiency of (a) PLA-1, and (b) PETG-1. This figure shows how the energy absorption key parameters are extracted.

softened. The alignment of the polymeric chains was lost, and the structures recovered most of their original shape. Figure 12 shows the results of the shape memory test of the samples. Results showed that the PETG-4 and PLA-4 have the lowest shape recovery ratio of 0.87 and 0.79, respectively. However, the rest of the samples have a shape recovery ratio higher than 0.90. PLA-1, Pla-2, and PLA-3 have the same level of shape recovery, i.e., 0.96 which is very promising shape recovery performance. PETG-3 has a shape recovery of 0.95 and PETG-1 and PETG-2 showed slightly less shape recovery by 0.92.

It should be noted that, for SMPs like semicrystalline PLA and amorphous PETG, the shape fixing and recovery mechanisms in CP vary due to their distinct molecular structures [24, 25]. In CP, conducted below T_g e.g., at room temperature, PLA's amorphous switching phase stores high strain energy with low configurationally entropy, anchored by its crystalline phase, leading to poor shape fixity as chains revert post-unloading, but rapid recovery upon heating. PETG, lacking crystalline domains, fixes temporary shapes via chain entanglement, resulting in a lower shape fixity ratio compared to PLA. However, PETG exhibits a high recovery ratio

Table 2. Comparison of the experimental and numerical energy absorption parameters of PETG samples.

	Parameters	$\in_y$	σ_y	$E_v(\in_d)$	σ_p	$\in_d$	SEA	$\eta(\in_d)$
Sample	Unit	$\left(\frac{mm}{mm}\right)$	(kPa)	$\left(\frac{kJ}{m^3}\right)$	(kPa)	$\left(\frac{mm}{mm}\right)$	$\left(\frac{kJ}{kg}\right)$	—
PETG-1	Experimental	0.04	78.23	18.34	78.99	0.25	0.11	0.24
	Numerical	0.05	81.39	18.01	77.02	0.25	0.11	0.23
PETG-2	Experimental	0.03	62.46	22.42	80.40	0.30	0.13	0.23
	Numerical	0.04	68.73	23.43	85.97	0.30	0.13	0.28
PETG-3	Experimental	0.03	77.25	17.91	79.29	0.24	0.11	0.27
	Numerical	0.03	83.20	21.49	82.64	0.27	0.13	0.29
PETG-4	Experimental	0.02	30.17	9.73	39.38	0.26	0.10	0.24
	Numerical	0.03	36.78	10.21	41.64	0.26	0.10	0.23

Table 3. Comparison of the experimental and numerical energy absorption parameters of PLA structures.

	Parameters	$\in_y$	σ_y	$E_v(\in_d)$	σ_p	$\in_d$	SEA	$\eta(\in_d)$
Sample	Unit	$\left(\frac{mm}{mm}\right)$	(kPa)	$\left(\frac{kJ}{m^3}\right)$	(kPa)	$\left(\frac{mm}{mm}\right)$	$\left(\frac{kJ}{kg}\right)$	—
PLA-1	Experimental	0.03	93.27	27.51	115.80	0.25	0.16	0.31
	Numerical	0.04	144.55	28.52	127.26	0.24	0.17	0.26
PLA-2	Experimental	0.03	85.25	24.14	92.47	0.28	0.14	0.29
	Numerical	0.04	108.50	31.12	112.19	0.30	0.18	0.26
PLA-3	Experimental	0.03	173.43	40.27	137.36	0.30	0.22	0.28
	Numerical	0.03	206.08	39.24	134.92	0.30	0.22	0.26
PLA-4	Experimental	0.03	59.90	9.99	45.86	0.22	0.10	0.38
	Numerical	0.03	52.03	12.58	47.66	0.26	0.12	0.35

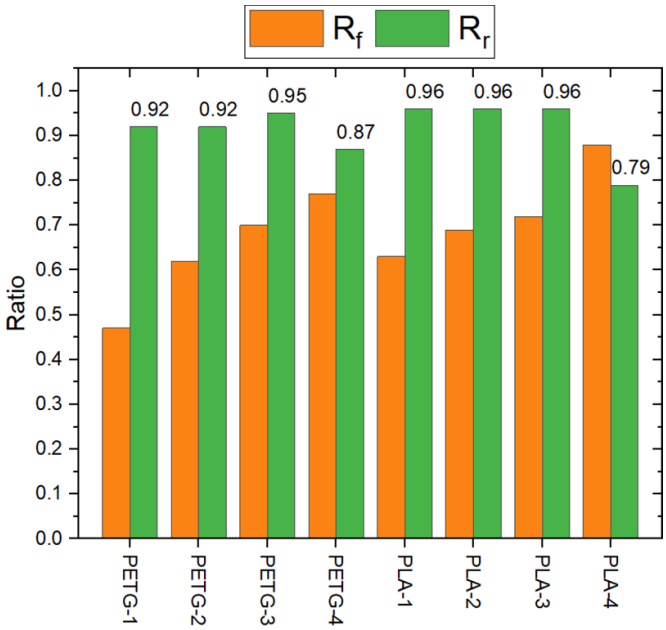

Figure 12. The shape memory test results for the PLA and PETG samples.

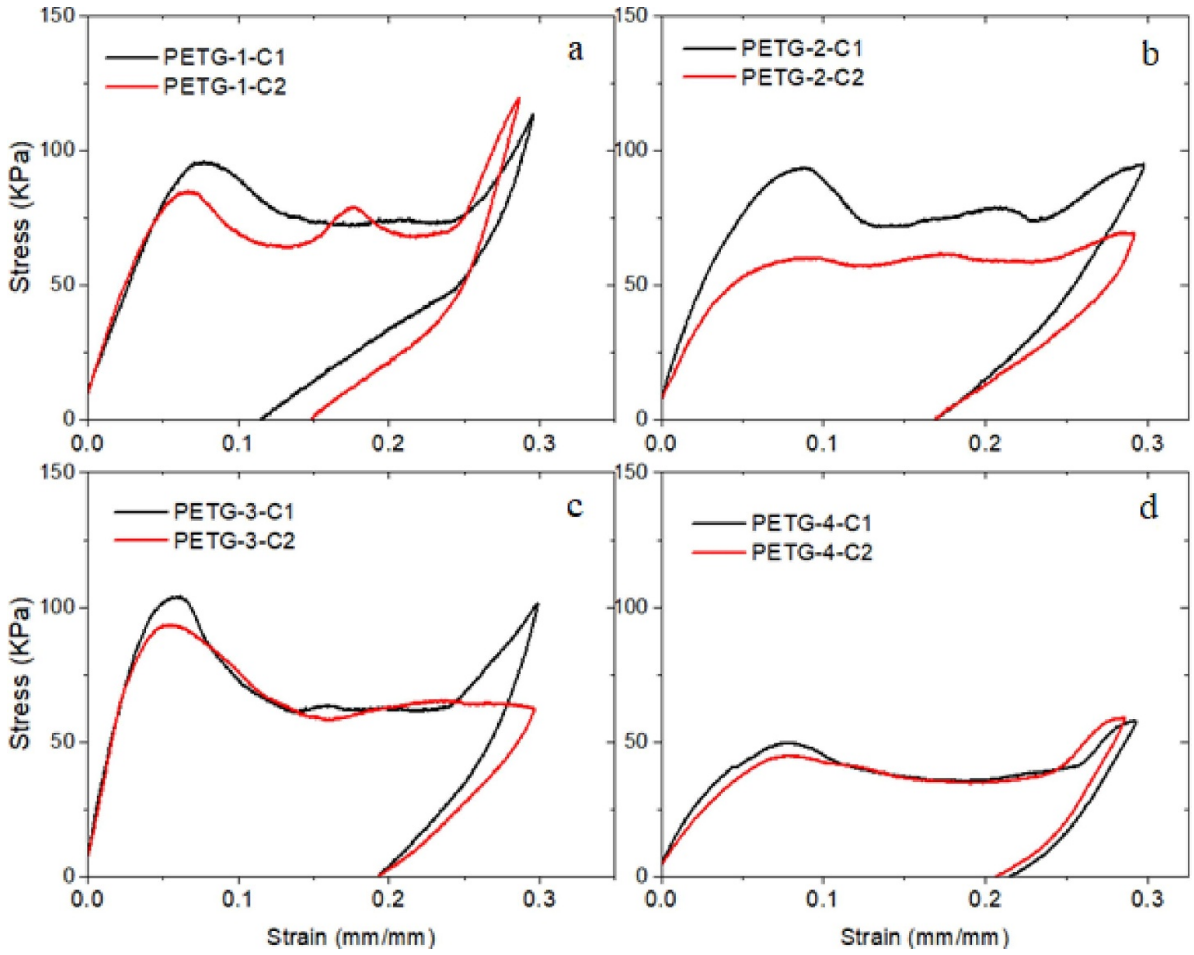

Figure 13. The stress–strain curves of the PETG samples for the first and second compression test. (a) PETG-1, (b) PETG-2, (c) PETG-3, and (d) PETG-4.

due to its ductility, though slightly lower than PLA, reflecting PLA's crystalline-driven recovery. Experimental results confirm that PLA samples, except PLA-4 which fractured, outperform PETG in recovery, while PETG's lower fixity enhances its suitability for flexible, reusable 4D-printed structures.

As mentioned before, reusability for a 4D printed structure is mandatory feature and without that there is no gain in using these types of structures. Here, to check the reusability of the 4D printed structure, all the recovered samples are again tested to see how their mechanical properties change compared to the intact samples. The stress–strain curve of the first and second cycle of compression test for PETG and PLA samples are presented in figures 13 and 14, respectively. Results in figure 13 show that the stress–strain curve of the first and second cycle compression test for PETG-1, PETG-3, and PETG4 are very similar, while for the PETG-2 the second cycle curve is different form the first cycle one. In all cases, the maximum stress is decreased in the second cycle, which can be interpreted as formation of plastic hinge and existence of unrecoverable deformation inside the structure.

Figure 14 shows that despite the PETG samples, for the PLA sample the difference between the first and second cycle is much. In all cases, the maximum load and the area under curve significantly decreased compared to the first cycle. The worst situation has been observed in the PLA-4 in which it does not tolerate any load in the second cycle. The main reason is that cracks and breakage were seen in this sample at the end of the first cycle of loading. Results of shape recovery test showed that PLA-4 recovered the intimal shape by 0.79 shape recovery ratio. However, the results of the second cycle compression test proved that this structure is no longer capable of bearing load. This is the main reason that besides the shape recovery properties of the 4D printed structures, their reusability should also be investigated to see if they can still bear loas.

To have a better comparison about these structures performance at the second cycle, the amount of absorbed energy in both cycles for PETG and PLA samples are presented in figures 15 and 16, respectively. Again, here it can be concluded that the difference between the absorbed energy in the first and second cycle for PLA samples are much higher than PETG samples. It means that the change in mechanical behavior of PETG samples after the second cycle is lower than PLA samples and they have better reusability compared to PLA samples. To quantify the reusability feature of the samples,

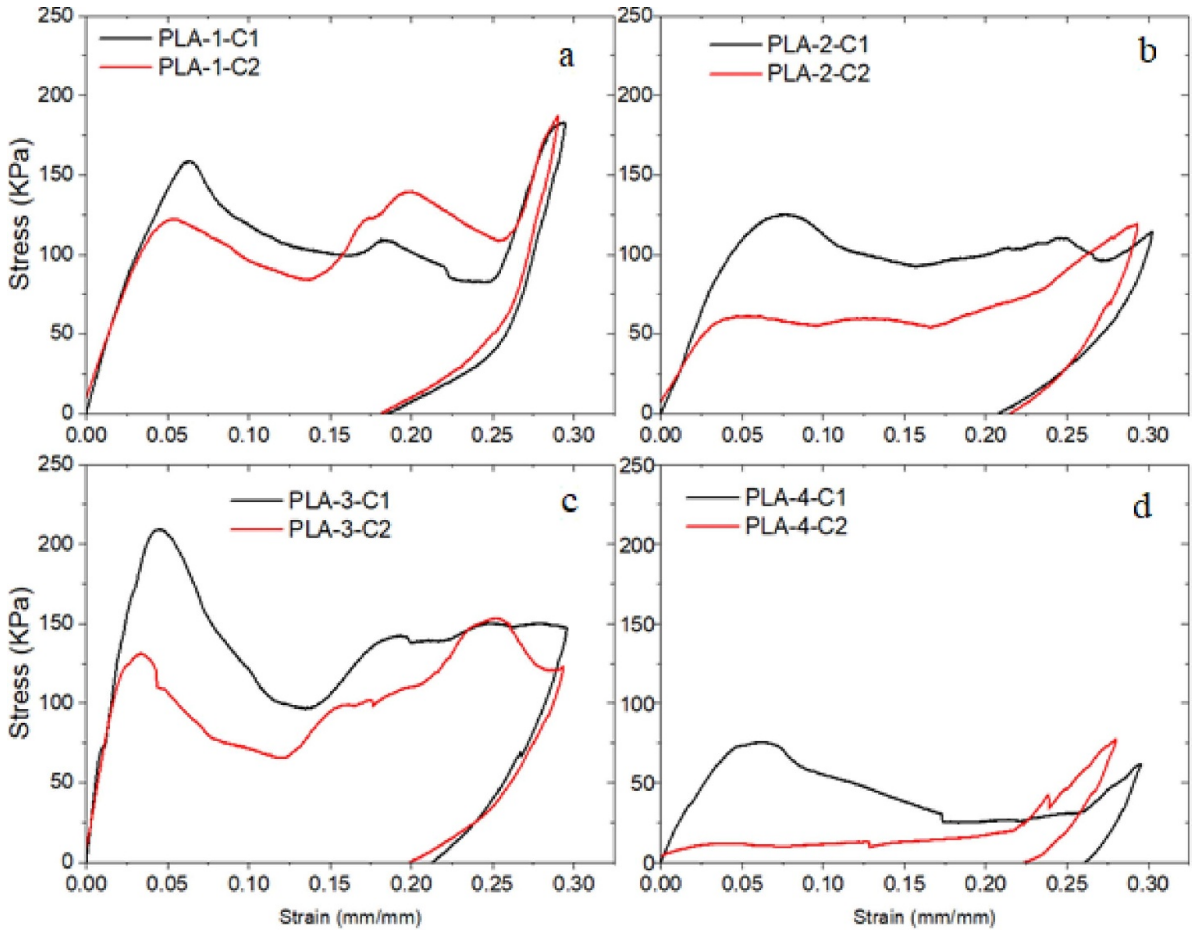

Figure 14. The stress–strain curves of the PLA samples for the first and second compression test. (a) PLA-1, (b) PLA-2, (c) PLA-3, and (d) PLA-4.

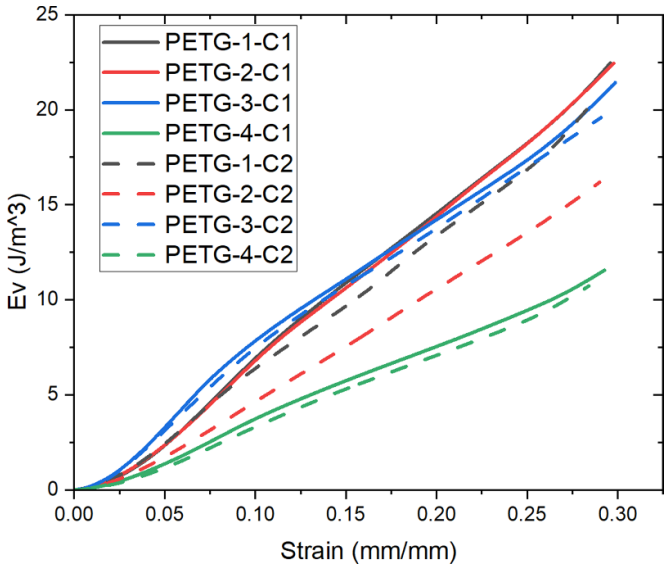

Figure 15. The absorbed per volume in the PLA sample for the first and second cycle of compression test.

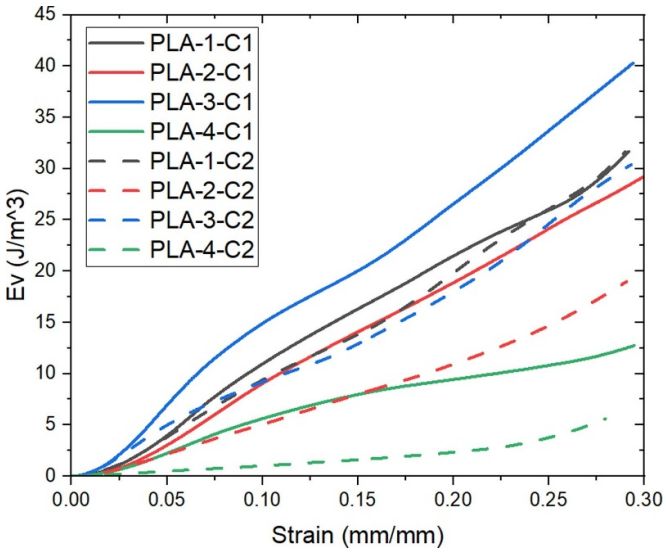

Figure 16. The absorbed per volume in the PLA sample for the first and second cycle of compression test.

their reliability factor is presented in figure 17. Their shape recovery ratio is also included to provide a better tool to compare these structures' performance.

As can be seen among the PLA samples, PLA-1 has the highest RF of 0.95, while PLA-4 has the lowest RF at 0.28. Among the PETG samples, PETG-3 has the highest RF value

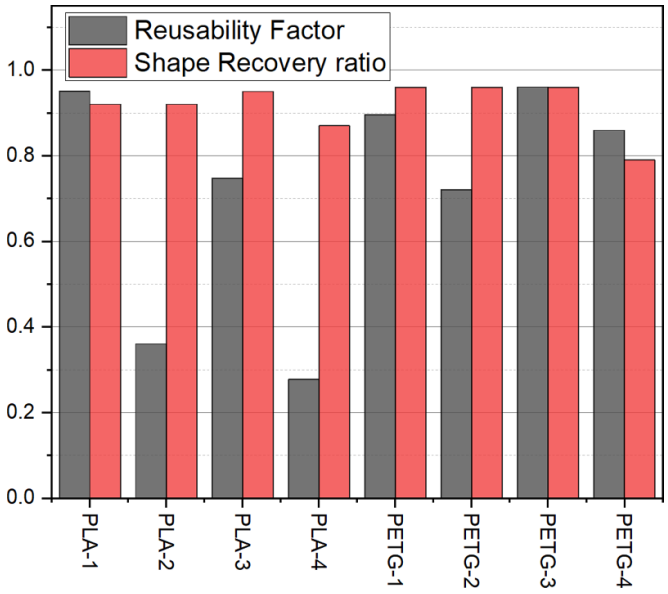

Figure 17. Reusability factor and shape recovery ratio of the 4D printed samples.

of 0.96, and PETG-2 has the lowest RF at 0.72. Overall, the RF of PETG samples is generally higher than that of PLA samples, suggesting that PETG is a more reusable material. However, while shape recovery ratios are promising across all samples, some exhibit low reusability due to significant mechanical degradation. For instance, PLA-2 and PLA-4 have shape recovery ratios of 0.92 and 0.87, respectively, but their RF values are below 0.5, indicating inadequate mechanical properties after recovery. This highlights a key limitation in evaluating 'smart' materials solely based on shape memory effects. Although high shape recovery qualifies these materials as 'smart' in terms of responding to external stimuli, practical applications require both shape recovery and mechanical durability. Thus, to design effective 4D-printed smart structures, both shape recovery and RFs must be considered to ensure the structures can withstand loads post-recovery, aligning with application-specific performance requirements.

4. Conclusion

In this study, the compression behavior, energy absorption, shape memory properties, and reusability of 4D-printed smart mechanical metamaterials were investigated. To this end, structures with four different configurations, including honeycomb, re-entrant, and two modified re-entrant designs, were fabricated and tested to analyze the impact of microstructure on the properties of the metamaterials. In addition, the 4D printed samples were fabricated using PLA and PETG, two commonly used SMPs. To simulate industrial application conditions, the shape memory test of the 4D printed structures was evaluated through CP-induced shape memory effect at RT. Furthermore, the compression behavior and complete shape memory cycle of the 4D printed structure were simulated using the finite element method, demonstrating a good agreement between the experimental and numerical findings. The findings indicate that PLA samples have higher mechanical performance compared to the PETG ones. Moreover, the pattern with NPR shows better energy absorption properties. For instance, the PETG-2 and PLA-3 showed the highest onset of densification among all the samples which is a desirable feature in energy absorption applications. Moreover, pattern 3 has higher mechanical properties compared to pattern 2 due to existence of additional vertical struts considered in this pattern. The PLA-4, which has the conventional honeycomb, showed the worst energy absorption performance and cracks have been observed at the end of loading.

After unloading, due to induced plastic strain in the structure, they just recovered some part of deformation elastically. Upon putting the samples in hot water, they recovered their original shapes. Results showed that all the samples have promising shape recovery. For instance, the PLA-1, PLA-2 and PLA-3 recovered their shape by 0.96 ratio and PETG1, PETG-2, and PETG-3 recovered their original shape by a ratio of more than 0.92. Both PLA-4 and PETG-4 showed a poor recovery due to excessive deformation and possible creaks in the structure during the loading.

In the next step, the recovered samples mechanical behavior is investigated to examine their reusability after shape recovery test. It is important to note that for a 4D printed smart structure that is designed for addressing real world applications, besides the high shape recovery, reusability is also crucial. Thus, a second cycle of compression test has been done for the record samples. Results showed that despite the promising recovery in the PLA samples, the mechanical response in the second cycle of compression test is significantly lower than the first cycle. However, in the PETG samples, the mechanical performance is slightly reduced, and they still can tolerate enough load. To measure the reusability quantitively, the RF has been defined, and results show that PETG samples have higher reusability in total. It should be noted that in this study, only two successive loading-recovery cycles were considered to compare the reusability of the printed samples. The results showed that PLA has poor reusability compared to PETG, making PETG a suitable replacement for PLA in 4D printing of smart load-bearing structures. It is also necessary to investigate the reusability and shape recovery properties of PETG samples after more cycles, which will be addressed in our future studies.

These results proved that despite most of studies about the 4D printed smart structure that only focused on the shape recovery of the structure, their reusability is also important. This study findings showed that PLA samples, despite their high shape recovery ratio, cannot tolerate load in the second cycle, thus they are not usable anymore. This fact is against the smart structure agenda.

Besides that, the analysis of PETG samples reveals a critical trade-off between SEA and RF in 4D-printed structures with auxetic unit cells. PETG-2, with its conventional re-entrant structure, achieves high SEA due to enhanced energy dissipation through localized buckling and densification but exhibits a lower RF, likely due to micro-cracking or plastic strain during deformation. Conversely, PETG-3, featuring a modified

re-entrant structure, demonstrates a higher RF, supported by PETG's toughness and optimized topology, which minimizes irreversible damage for superior cyclic performance, though at the expense of lower SEA. These findings emphasize that while auxeticity enhances energy absorption in both designs, it can lead to irreversible deformation in conventional structures, whereas modified designs prioritize recoverable strain for reusability. By balancing SEA and RF, this study offers a framework for selecting materials and topologies to meet specific application needs in 4D printing.

This is the first paper investigating the behavior of 4D materials and structures both computationally and experimentally. This integrative computational and experimental work will open new further research on not only 4D printing of reusable metamaterials but also digital twinning of metamaterials.

Data availability statement

All data that support the findings of this study are included within the article (and any supplementary files).

Acknowledgment

This study was supported by the Scientific and Technological Research Council of Turkey (TÜBİTAK) under Grant No. 221M067, which provided support to Ali Fallah, Qandeel Saleem and Bahattin Koc. Giulia Scalet acknowledges support from Italian Ministry of University and Research within the Call related to the scrolling of the final rankings of the PRIN 2022 call (Project StArT No 2022WFJ795, CUP F53C24001030001).

Conflict of interest

All authors certify that they have no affiliations with or involvement in any organization or entity with any financial interest or non-financial interest in the subject matter or materials discussed in this manuscript.

ORCID iDs

Ali Fallah https://orcid.org/0000-0002-7744-4246
Qandeel Saleem https://orcid.org/0000-0003-4444-4722
Giulia Scalet https://orcid.org/0000-0001-7683-566X
Bahattin Koc https://orcid.org/0000-0001-9073-8516

References

[1] Bodaghi M, Serjouei A, Zolfagharian A, Fotouhi M, Rahman H and Durand D 2020 Reversible energy absorbing meta-sandwiches by FDM 4D printing *Int. J. Mech. Sci.* **173** 105451
[2] Yazdani Sarvestani H *et al* 2018 3D printed architected polymeric sandwich panels: energy absorption and structural performance *Compos. Struct.* **200** 886–909
[3] Dara A, Mertens A J, Gunji B and Bahubalendruni M V A R 2025 Quasi-static and dynamic response of open lattice structures for enhanced plateau stresses: simulation and experiment validation *Mater. Today Commun.* **44** 111953
[4] Calpana R, Ashok D, Prasanna A, Kasireddy S R and Raju Bahubalendruni M V A 2025 Experimental characterization and numerical investigation on different conformal lattice structures for specific energy absorption under quasi-static and dynamic loading *Int. J. Prot. Struct.* (https://doi.org/10.1177/20414196251321495)
[5] Rahman H, Yarali E, Zolfagharian A, Serjouei A and Bodaghi M 2021 Energy absorption and mechanical performance of functionally graded soft-hard lattice structures *Materials* **14** 1366
[6] Kolken H M A and Zadpoor A A 2017 Auxetic mechanical metamaterials *RSC Adv.* **7** 5111–29
[7] Choudhry N K, Panda B and Kumar S 2022 In-plane energy absorption characteristics of a modified re-entrant auxetic structure fabricated via 3D printing *Composites B* **228** 109437
[8] Choudhry N K, Panda B and Kumar S 2023 Enhanced energy absorption performance of 3D printed 2D auxetic lattices *Thin-Walled Struct.* **186** 110650
[9] Li T, Chen Y, Hu X, Li Y and Wang L 2018 Exploiting negative Poisson's ratio to design 3D-printed composites with enhanced mechanical properties *Mater. Des.* **142** 247–58
[10] Teng X C, Ren X, Zhang Y, Jiang W, Pan Y, Zhang X G, Zhang X Y and Xie Y M 2022 A simple 3D re-entrant auxetic metamaterial with enhanced energy absorption *Int. J. Mech. Sci.* **229** 107524
[11] Attard D and Grima J N 2012 A three-dimensional rotating rigid units network exhibiting negative Poisson's ratios *Phys. Status Solidi b* **249** 1330–8
[12] Gatt R, Mizzi L, Azzopardi J I, Azzopardi K M, Attard D, Casha A, Briffa J and Grima J N 2015 Hierarchical auxetic mechanical metamaterials *Sci. Rep.* **5** 8395
[13] Grima J N *et al* 2016 Auxetic perforated mechanical metamaterials with randomly oriented cuts *Adv. Mater.* **28** 385–9
[14] Jiang Y and Li Y 2018 Novel 3D-printed hybrid auxetic mechanical metamaterial with chirality-induced sequential cell opening mechanisms *Adv. Eng. Mater.* **20** 1700744
[15] Attard D, Calleja D and Grima J N 2017 Out-of-plane doming behaviour from constrained auxetics *Smart Mater. Struct.* **27** 015020
[16] Grima J N, Gatt R, Alderson A and Evans K E 2005 On the potential of connected stars as auxetic systems *Mol. Simul.* **31** 925–35
[17] Lim T C 2016 A 3D auxetic material based on intersecting double arrowheads *Phys. Status Solidi b* **253** 1252–60
[18] Zhang J, Lu G and You Z 2020 Large deformation and energy absorption of additively manufactured auxetic materials and structures: a review *Composites B* **201** 108340
[19] Dara A *et al* 2022 Numerical and experimental investigations of novel nature inspired open lattice cellular structures for enhanced stiffness and specific energy absorption *Mater. Today Commun.* **31** 103286
[20] Ning F *et al* 2015 Additive manufacturing of carbon fiber reinforced thermoplastic composites using fused deposition modeling *Composities B* **80** 369–78
[21] Carneiro O S, Silva A and Gomes R 2015 Fused deposition modeling with polypropylene *Mater. Des.* **83** 768–76
[22] Wittbrodt B and Pearce J M 2015 The effects of PLA color on material properties of 3-D printed components *Addit. Manuf.* **8** 110–6
[23] Turner B N, Strong R and Gold S A 2014 A review of melt extrusion additive manufacturing processes: I. Process design and modeling *Rapid Prototyp. J.* **20** 192–204

[24] Fallah A *et al* 2023 4D printing of continuous fiber-reinforced electroactive smart composites by coaxial additive manufacturing *Compos. Struct.* **316** 117034
[25] Nejatpour M, Fallah A and Koc B 2024 An overview of 4D printing of smart multifunction continuous fiber-reinforced composites: recent advances and novel applications *Adv. Compos. Hybrid Mater.* **7** 133
[26] Tibbits S 2014 4D printing: multi-material shape change *Arch. Des.* **84** 116–21
[27] Namvar N, Zolfagharian A, Vakili-Tahami F and Bodaghi M 2022 Reversible energy absorption of elasto-plastic auxetic, hexagonal, and AuxHex structures fabricated by FDM 4D printing *Smart Mater. Struct.* **31** 055021
[28] Xin X, Liu L, Liu Y and Leng J 2020 4D printing auxetic metamaterials with tunable, programmable, and reconfigurable mechanical properties *Adv. Funct. Mater.* **30** 2004226
[29] Dong K, Wang Y, Wang Z, Qiu W, Zheng P and Xiong Y 2023 Reusability and energy absorption behavior of 4D printed continuous fiber-reinforced auxetic composite structures *Composites A* **169** 107529
[30] Sun G, Wang J, Wang K, Baghani M, Peng Y and Rao Y 2023 Repeatable compressive functionality of 3D printed shape-memory thin-walled corrugated structures *Int. J. Mech. Sci.* **257** 108552
[31] Zhang D, Liu L, Lan X, Li F, Liu Y and Leng J 2023 Experimental study on nonlinearity of unidirectional carbon fibre-reinforced shape memory polymer composites *Composites A* **166** 107372
[32] Farrokhabadi A, Mahdi Ashrafian M, Behravesh A H and Kaveh Hedayati S 2022 Assessment of fiber-reinforcement and foam-filling in the directional energy absorption performance of a 3D printed accordion cellular structure *Compos. Struct.* **297** 115945
[33] Zhang D, Li M, Qiu N, Yang J, Wu C, Steven G, Li Q and Fang J 2024 4D-printed reusable metamaterial via shape memory effect for energy dissipation *Int. J. Mech. Sci.* **275** 109309
[34] Xin X, Liu L, Liu Y and Leng J 2019 Mechanical models, structures, and applications of shape-memory polymers and their composites *Acta Mech. Solida Sin.* **32** 535–65
[35] Li G and Wang A 2016 Cold, warm, and hot programming of shape memory polymers *J. Polym. Sci. B* **54** 1319–39
[36] Fallah A, Saleem Q and Koc B 2024 Assessment of mechanical properties and shape memory behavior of 4D printed continuous fiber-reinforced PETG composites *Composites A* **181** 108165
[37] Chapkin W A, Simone D L, Frank G J and Baur J W 2021 Mechanical behavior and energy dissipation of infilled, composite Ti-6Al-4V trusses *Mater. Des.* **203** 109602
[38] Avalle M, Belingardi G and Montanini R 2001 Characterization of polymeric structural foams under compressive impact loading by means of energy-absorption diagram *Int. J. Impact Eng.* **25** 455–72
[39] Alomarah A, Masood S H, Sbarski I, Faisal B, Gao Z and Ruan D 2020 Compressive properties of 3D printed auxetic structures: experimental and numerical studies *Virtual Phys. Prototyp.* **15** 1–21
[40] Boatti E, Scalet G and Auricchio F 2016 A three-dimensional finite-strain phenomenological model for shape-memory polymers: formulation, numerical simulations, and comparison with experimental data *Int. J. Plast.* **83** 153–77
[41] Luo H C, Ren X, Zhang Y, Zhang X Y, Zhang X G, Luo C, Cheng X and Xie Y M 2022 Mechanical properties of foam-filled hexagonal and re-entrant honeycombs under uniaxial compression *Compos. Struct.* **280** 114922
[42] Farrokhabadi A, Veisi H, Gharehbaghi H, Montesano J, Behravesh A H and Hedayati S K 2023 Investigation of the energy absorption capacity of foam-filled 3D-printed glass fiber reinforced thermoplastic auxetic honeycomb structures *Mech. Adv. Mater. Struct.* **30** 758–69